Diagnostics-oriented Model for Automotive SCR-ASC

Kaushal K. Jain[1], Peter H. Meckl[2], Pingen Chen[3], and Kuo Yang[4]

[1,2] *School of Mechanical Engineering, Purdue University, West Lafayette, IN 47907*
jain172@purdue.edu
meckl@purdue.edu

[3,4] *Department of Mechanical Engineering, Tennessee Tech University, Cookeville, TN 38505*
pchen@tntech.edu
kyang42@students.tntech.edu

ABSTRACT

This paper presents a diagnostics-oriented aging model for combined Selective Catalytic Reduction (SCR) and Ammonia Slip Catalyst (ASC) system, along with a model-based on-board diagnostic (OBD) method applied to both test-cell data and on-road data from commercial trucks. The key challenge with model development was unavailability of NOx and NH_3 measurements between SCR and ASC. Since it would have been very difficult to calibrate both SCR and ASC dynamics without any measurements between SCR and ASC, therefore ASC was modeled using static look-up tables to determine ASC's NH_3 conversion efficiency and its selectivity to NOx and N_2O as a function of temperature and flow rate. The traditional three-state single-cell ordinary differential equation (ODE) model was used for SCR. Hot Federal Test Procedure (hFTP) was used to calibrate the model. Cold FTP (cFTP) and Ramped Mode Cycle (RMC) were used for validation. Results show that the SCR-ASC model can capture the aging signatures in tailpipe NOx, NH_3, and N_2O reasonably well for cFTP, hFTP, and RMC cycles in the test-cell data. After slight re-calibration and combining with a simple model for commercial NOx sensor's cross-sensitivity to NH_3, the model works reasonably well for on-road data from commercial trucks. A model-based on-board diagnostic (OBD) method has been presented with enable conditions designed to detect operating conditions suitable for detecting aging signatures, while minimizing false positives and false negatives. The OBD method is applied to both test-cell and real-world truck data with commercial NOx sensors. Results on test-cell data demonstrate the challenges of robust SCR monitoring even on the limited data set used in this work. The model-based enable conditions are shown to be robust but extremely restrictive as the OBD gets enabled at very few points in the test-cell data. Application on truck data showed that the proposed OBD method can be implemented on commercial trucks with limited sensors. In the truck data, the enable conditions were satisfied on many more points than the test-cell data. Results on truck data show encouraging trends between relative degradation level and the number of miles on four trucks. In future work, these trends will be validated using more data from commercial trucks with known aging levels.

1. INTRODUCTION

Selective Catalytic Reduction (SCR) and Ammonia Slip Catalyst (ASC) are important components of the diesel engine aftertreatment. SCR reduces the engine-out NOx into harmless N_2 and H_2O using NH_3, which is injected into the system as Diesel Exhaust Fluid or DEF. ASC is responsible for oxidizing SCR-out NH_3. Thus, the SCR-ASC system minimizes tailpipe NOx and NH_3 emissions.

A major challenge with the SCR-ASC system is degradation or aging of the SCR catalyst with time, which leads to an increase in tailpipe NOx emissions. Therefore, it is important for diesel-engine vehicles to be equipped with effective model-based on-board diagnostics (OBD), which can monitor and report catalyst degradation before it degrades beyond acceptable levels. An important step towards designing model-based OBD is to develop a diagnostics-oriented model for SCR-ASC.

To the best of the authors' knowledge, most existing aging models and diagnostic strategies have only been demonstrated in simulation. A few that have demonstrated hardware results have used a catalyst that was aged in a controlled environment through accelerated hydrothermal aging. Also, most existing diagnostics-oriented models have not considered the presence of ASC. These gaps are elaborated as follows:

https://doi.org/10.36001/IJPHM.2023.v14i3.3129

1. **On-road vs test-cell/simulations:** Environmental Protection Agency (EPA) and California Air Resource Board (CARB) have rigorous and effective test-cell routines to certify vehicles. However, their findings, from logging over a month's on-road OBD data from 68 trucks, show that there is significant discrepancy between real-world and test-cell emissions (Emissions Compliance & Science Division, 2018 (accessed Nov 30, 2021)) (Romijn & Kumar, 2018 (accessed Nov 30, 2021)) ("CARB approves heavy-duty OBD amendments, adopts REAL NOx and CO2 tracking", 2018 (accessed Nov 30, 2021)). This challenge is also reflected in the academic literature, cited later in this section, where most aging models and diagnostic strategies have only been demonstrated in simulation. A few that have demonstrated hardware results have used a catalyst that was aged in a controlled environment through accelerated hydrothermal aging. Although this is a good simulation, it is still not a perfect replication of on-road aging.
2. **Intrusive vs non-intrusive**: There are patents from industry that have proposed diagnostic algorithms designed to work under on-road conditions. However, most of these algorithms are intrusive. Since the most recent regulations contain stringent restrictions on intrusive diagnostics, it is important to develop non-intrusive methods that can work under on-road conditions.
3. **Commercial aftertreatment system:** To the best of our knowledge, most existing literature has not considered the presence of ASC or absence of tailpipe NH_3 sensors in commercial aftertreatment systems. Therefore, diagnostic algorithms that can monitor the SCR-ASC system using a commercial tailpipe NOx sensor must be developed.

Our objective is to contribute towards filling the aforementioned gaps by developing model-based non-intrusive diagnostics for SCR-ASC that can work with commercial NOx sensors.

Cummins Inc. has generously provided on-road data for four trucks, and test-cell data for cold FTP, hot FTP, and Ramped Mode Cycle (RMC) for degreened and aged catalysts. The first task in the project is to develop diagnostics-oriented aging models for SCR-ASC using test-cell data, which will then be used to develop the model-based on-board diagnostic method.

A very popular approach to model catalyst degradation is to scale some parameter in a control-oriented SCR model by an "aging factor". The aging factor decreases from 1 for a degreened catalyst to, say 0.5, for a catalyst at end-of-useful-life (EUL). This aging factor can then be estimated using a model-based estimator to monitor catalyst degradation. Papers from Junmin Wang's research group have modeled aging by scaling the catalyst NH_3 storage capacity, which is estimated using a Lyapunov-based nonlinear observer to report catalyst age (Chen & Wang, 2016; Ma & Wang, 2017). Both the aging model and the observer in these papers are based on the four-state model in (Hsieh, 2010) and (Devarakonda, Parker, Johnson, Strots, & Santhanam, 2008). Schär et al. introduced the popular three-cell three-state model for SCR in (Schär, Onder, Geering, & Elsener, 2004). Using this model, Hu et al. simulated catalyst degradation by scaling the NOx reduction rate (Hu, Zeng, Wei, & Yan, 2017). In another paper, they scaled the NH_3 storage capacity, which is estimated using an Extended Kalman Filter (EKF) (Hu, Zeng, & Wei, 2018). Stadlbauer et al. scaled the NH_3 adsorption reaction rate in Schär et al's model to capture catalyst degradation. The two-cell three-state model by Upadhyay et al. is another popular control-oriented model for urea-SCR (Upadhyay & Van Nieuwstadt, 2002). Jiang et al. have modeled aging by scaling the NH_3 storage capacity in Upadhyay et al's model. Degradation is reported by estimating the storage capacity using Unscented Kalman Filter (UKF) (Jiang, Yan, & Zhang, 2019). It should be noted that none of these aging models have been validated on an actual aged catalyst yet. Simulation results for all the observers show good performance for aging factor estimation. It should be noted that the observers in all these papers rely on accurate tailpipe NOx and NH_3 feedback, except (Ma & Wang, 2017), who have presented an additional observer that can work with just tailpipe NOx feedback.

Instead of capturing age through a single parameter, an alternate approach is to perform separate calibrations for degreened and aged catalysts as done in (Surenahalli, 2013). This resulted in different values for all parameters across degreened and aged catalysts.

Recent publications, by Daya et al. from Cummins Inc., on high-fidelity aging models report that there are various types of active sites where NH_3 storage happens: Bronsted acid sites, Cu sites and physisorbed NH_3 sites. Since the impact of aging on reaction rates and density of active sites could be different for different sites, it is recommended that at least two sites should be used in aging models (Daya et al., 2020; Daya, Desai, & Vernham, 2018).

Matsumoto et al. have published the most promising paper on SCR OBD so far as it presents an OBD method that considers the presence of ASC, works with the commercial tailpipe NOx sensor, and is demonstrated for real-world driving conditions (Matsumoto, Furui, Ogiso, & Kidokoro, 2016). A two-cell SCR model and a single-cell ASC model are calibrated individually using SCR-in, SCR-out, and ASC-out measurements. Both SCR and ASC models are Differential Algebraic Equation (DAE) models, except that a discretized equation is used to calculate NH_3 storage and the equations for tailpipe NOx and NH_3 are slightly different from the common Continuous Stirred Tank Reactor (CSTR) assumption-

based equations. Each reaction is calibrated individually using steady-state tests. The SCR-ASC model is calibrated for both fresh and aged catalysts. The fresh and aged catalyst models are used to calculate the worst acceptable performance (highest possible value that could be reported by tailpipe NOx sensor for a good catalyst) and the best unacceptable performance (lowest possible value that could be reported by tailpipe NOx sensor for an aged catalyst), respectively at each operating point. OBD is enabled only when the tailpipe NOx sensor value for the best unacceptable performance is more than that for the worst acceptable performance by a threshold. The OBD can only do binary classification. It can not report multiple aging levels. The OBD is shown to work with reasonable In-Use Performance Monitor Ratio (IUMPR) for the New European Driving Cycle and about ten other driving patterns which customers actually drive. IUMPR is defined by the California Air Resources Board (CARB) as the ratio of the number of times the OBD, also referred to as the "diagnostic monitor" or "monitor", is active during vehicle operation to the number of "driving events" during vehicle operation. In the context of IUMPR, CARB defines a "driving event" as a trip that begins either with an engine start or at the end of a four-hour-long continuous engine-on operation, and ends with either engine stop or after four hours of continuous engine-on operation. The workflow in this paper is very similar to our project. However, an additional challenge for us is that we don't have access to SCR-out measurements. Also, the aged catalyst in this work was prepared via accelerated aging in an electrical furnace, whereas the aged catalyst in our work degraded on the road.

To summarize, most existing literature on SCR diagnostics have either shown results on simulation or on test-cell data with hydrothermally aged catalyst in the lab. **The key contributions of this paper are:**

1. Observations about the effects of real-world catalyst degradation on tailpipe NOx, NH_3, and N_2O are presented based on data from test-cell experiments on a degreened and an aged catalyst, which degraded to end-of-useful-life (EUL) on the road.
2. Insights from the test-cell data and observations from on-road truck data are then used to describe challenges with designing model-based on-board diagnostics that could work for the aftertreatment system on commercial trucks.
3. A novel diagnostics-oriented SCR-ASC model is presented, which is shown to work reasonably well, for the purpose of model-based OBD, for both test-cell data and on-road data from commercial trucks. The model is calibrated on the hot FTP cycle and validated on the cold FTP and RMC cycles in test-cell data. After slight recalibration and combining with a simple model for NOx sensor's cross-sensitivity to NH_3, the model works reasonably well for the purpose of model-based OBD on the truck data as well.
4. A complete model-based OBD method is presented with model-based enable conditions designed to detect operating conditions suitable for diagnostics, while minimizing false positives and false negatives due to model uncertainties and NOx sensor's cross-sensitivity to NH_3. The method was applied to both test-cell data and real-world truck data with commercial NOx sensors. The method is shown to be robust to cross-sensitivity but the enable conditions are very restrictive as they are satisfied at very few points in the test-cell data. The method is shown to be implementable on commercial trucks with limited sensors and the results on truck-data are encouraging but could not be validated yet as the aging levels of the catalysts on these trucks are unknown.

The paper is organized as follows. First, the important details and observations from the test-cell and truck data are presented. Based on these, the model requirements are laid out, which is followed by a detailed description of SCR and ASC model development, calibration, and validation. The paper concludes with results from applying model-based OBD on both test-cell and truck data as foundation for future work.

2. DATA

2.1. Test-cell Data

The test-cell data for this paper consists of four data-sets. These data-sets contain emissions data for a degreened (DG) and an end-of-useful-life (EUL) aftertreatment system, for three drive cycles: 1) Cold Federal Test Procedure (cFTP), 2) Hot Federal Test Procedure (hFTP), and 3) Ramped Mode Cycle (RMC). The key components of the aftertreatment system are Diesel Oxidation Catalyst (DOC), Diesel Particulate Filter (DPF), SCR, and ASC. Each data-set contains the following measurements: Engine torque; Engine speed; Diesel Exhaust Fluid (DEF) injection rate; Engine-out NOx; DOC-out NO, NO_2; Tailpipe NOx, NH_3, N_2O; DOC-in, DOC-out, SCR-in, ASC-out temperature; Exhaust flow rate. The exhaust layout, with the sensors available in test-cell, is shown in Figure 1. Table 1 shows the dimensions of the exhaust components.

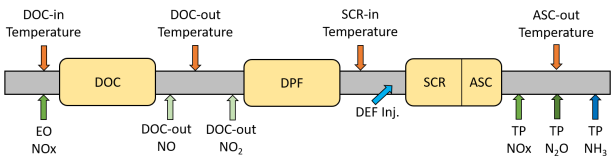

Figure 1. Exhaust layout with the sensors available in test-cell

	DOC	DPF	SCR	ASC
Diameter (in)	13	13	13	13
Length (in)	4	7	9.5	2

Table 1. Dimensions of the key aftertreatment components in Cummins aftertreatment system used in this work.

2.1.1. Comparing operating conditions across drive cycles

Figure 2 shows the SCR-inlet quantities for cFTP, hFTP, and RMC cycles.

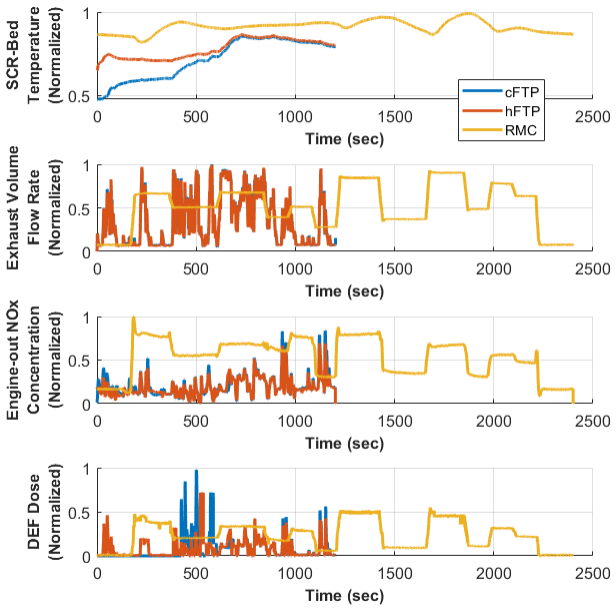

Figure 2. Input signals for the three drive cycles (all signals are normalized by dividing by their maximum value across the three drive cycles).

Some observations regarding the operating conditions across the three drive cycles are as follows:

1. **SCR-bed temperature:** hFTP has higher temperature than cFTP during the first 600 seconds and both have identical temperature after 600 seconds. RMC has higher temperature than both cFTP and hFTP throughout the cycle.
2. **Engine-out (EO) NOx and Exhaust Flow Rate:** Both cFTP and hFTP cycles have transient changes in engine torque and speed, which lead to transient engine-out NOx and exhaust flow rate. Engine-out NOx and flow rate are identical for cFTP and hFTP throughout the cycle. RMC has step changes in engine torque and speed, leading to step changes in engine-out NOx and flow rate. The range of engine-out NOx and flow rate is similar across the three cycles
3. **Urea Dosing:** Four distinct observations were made about urea-dosing profiles for cFTP and hFTP cycles across different time ranges. From $t = 0$ to $t = 424$ sec, there is zero DEF dosing for cFTP unlike hFTP, which has non-zero dosing. From $t = 424$ to $t = 520$ sec, cFTP has higher dosing than hFTP. From $t = 520$ to $t = 600$ sec, a distinct step DEF dosing profile is observed for both cFTP and hFTP at different times. In the last phase beyond $t = 600$ sec, both cFTP and hFTP have almost the same dosing profile. RMC again has step changes in urea dosing, but the range is similar to the two FTP cycles.
4. **Initial NH_3 storage:** The exact amount of NH_3 at the start of each cycle is not known. However, the following protocol was followed for the three cycles:
   - **FTP Cycles**: Run two cycles of running a preparation FTP followed by a 20-minute soak. This is followed by another preparation FTP, followed by an overnight cold soak. The next FTP cycle is labeled as cFTP. This is followed by another soak 20-minute soak, and the FTP after that is labeled as hFTP.
   - **RMC Cycle**: A preparation RMC is followed by the measured RMC.

2.1.2. Aging Signatures

The aged catalyst in the test-cell data was assumed to be degraded to EUL level on the road. As shown in Figure 3, both degreened and EUL aftertreatment systems were operated under the exact same operating conditions for each cycle. Therefore, the difference in DOC-out and tailpipe (TP) signals can be attributed to aging. And these differences in DOC-out and tailpipe signals due to aging are called aging signatures.

The following aging signatures were observed in the test-cell data:

1. **DOC-out NO, NO_2:** Engine-out NOx is rich in NO, leading to an NO_2/NO ratio less than 1. Since SCR's deNOx efficiency improves if NO_2/NO ratio is close to 1, DOC's job is to oxidize NO to NO_2. Aftertreatment aging leads to a decline in DOC performance, which decreases the DOC-out NO_2/NO ratio. This was clearly observed for all three cycles as shown in Figure 4.
2. **Tailpipe N_2O:** Figure 5 shows tailpipe N_2O for the three cycles. EUL catalyst produced significantly higher N_2O than degreened for cFTP and hFTP, from around 600 sec to 1000 sec. This could be because of higher SCR-out NH_3 slip from the EUL catalyst, during those times, that gets converted to tailpipe N_2O by the ASC. Both catalysts produced almost identical amount of tailpipe N_2O

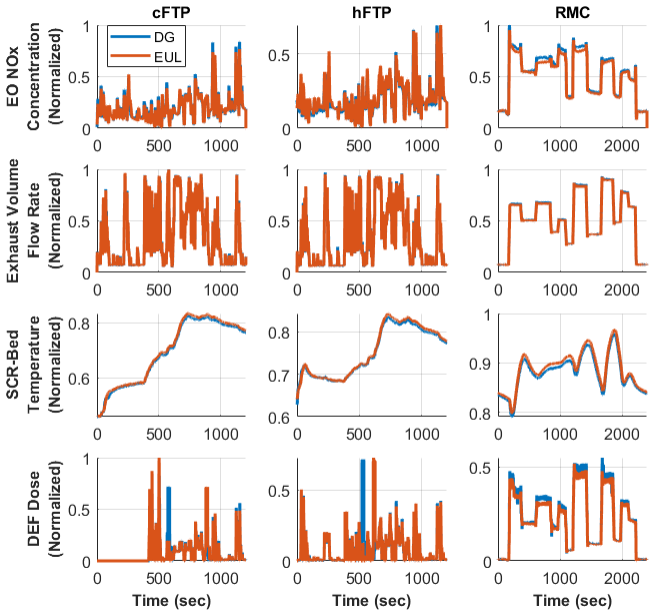

Figure 3. Input signals for both degreened and EUL catalysts for the three drive cycles.

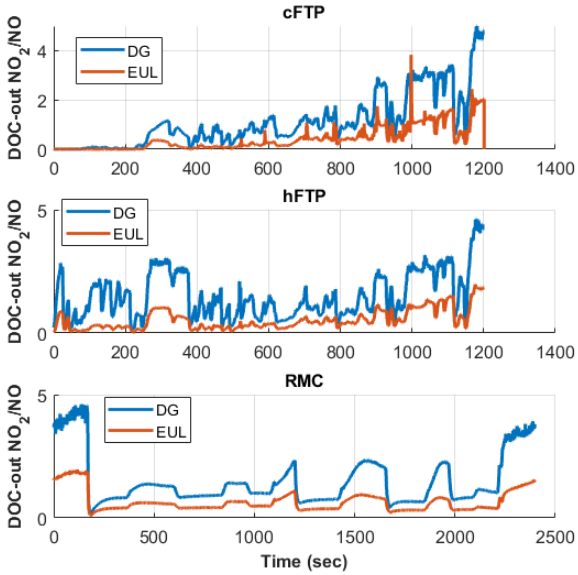

Figure 4. DOC-out NO_2/NO for both degreened and EUL catalysts for the three drive cycles.

for the RMC cycle, with degreened catalyst producing slightly higher N_2O than EUL.

3. **Tailpipe NH_3:** Tailpipe NH_3 slip for all three cycles was very low because of the presence of ASC. As shown in Figure 6, hFTP showed slightly higher NH_3 slip (around 5 ppm) for the EUL catalyst.
4. **Tailpipe NOx:** Aging is expected to cause a decline in SCR performance, leading to lower deNOx or higher tailpipe NOx. However, the test-cell data showed that tailpipe NOx for the EUL catalyst may not be higher than the degreened catalyst at all times. Only five segments of data, shown in Figure 7, across the three cycles, showed reasonably higher (>10 ppm) tailpipe NOx for the EUL catalyst.

Following are the key take-aways from these observations:

1. The effect of aging on DOC performance is evident from the smaller DOC-out NO_2/NO ratio for the EUL catalyst across the three cycles.
2. The decline in SCR performance due to aging is expected to result in an increase in tailpipe NOx and NH_3 slip. However, due to the presence of ASC, tailpipe NH_3 stays low at all times and the increase in SCR-out NH_3 slip manifests through an increase in tailpipe N_2O.
3. Only five aging signatures in tailpipe NOx, i.e. reasonably higher (>10 ppm) tailpipe NOx for the EUL catalyst than the degreened catalyst, across the three drive cycles demonstrate that not all operating conditions will reveal the catalyst age. This establishes the importance of picking the right operating conditions to enable the diagnostics algorithm.

2.2. Truck Data

The truck data consists of four "day-files". Each day-file has on-road data collected using commercial on-board sensors during 24-hour drive of a truck. The four day-files are for four different trucks with 271k, 422k, 484k, and 711k miles on them. Each day file contains several measurements such as: Engine torque; Engine speed; Truck speed; Cruise-control information; DPF-regeneration information; Diesel Exhaust Fluid (DEF) injection; Engine-out NOx; Tailpipe NOx; DOC-in, SCR-in, ASC-out temperatures; Exhaust flow rate. The aftertreatment system on these trucks is same as the one used to collect test-cell data. The exhaust layout, with the sensors available on these trucks, is shown in Figure 8.

2.2.1. Operating conditions

Figure 9 shows a 7-minute segment of truck data. Differences in accelerator pedal position, altitude, and ambient temperature demonstrate that each driver has their own driving style, and every truck could be driven under different road, traffic, and weather conditions. Therefore, the operating conditions vary significantly across the four trucks.

Table 2 lists the minimum, maximum, and average values of engine-out NOx, exhaust flow, temperature and urea dosing over the entire day file for each truck. Notice that the average values of exhaust flow rate and temperature are very similar

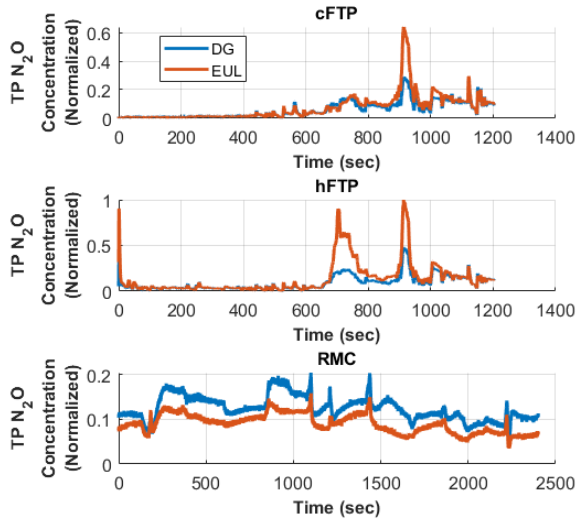

Figure 5. Tailpipe N_2O for degreened and EUL catalysts for the three drive cycles.

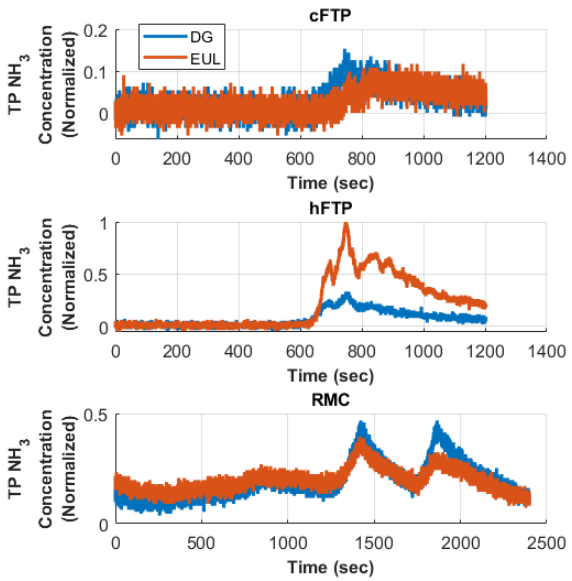

Figure 6. Tailpipe NH_3 for degreened and EUL catalysts for the three drive cycles.

across the four trucks, but the ranges and average values of engine-out NOx and urea dose vary across the four trucks.

		Truck 1	Truck 2	Truck 3	Truck 4
EO NOx (ppm)	min	0	0	0	0
	avg	403	408	573	490
	max	1371	1203	2237	1647
Flow Rate (m^3/sec)	min	0	0	0	0
	avg	0.35	0.27	0.35	0.30
	max	0.61	0.65	0.77	0.67
SCR Bed Temperature (^{o}C)	min	50	72	44	113
	avg	244	243	253	241
	max	314	557	354	374
Urea Dose (ml/sec)	min	0	0	0	0
	avg	0.34	0.25	0.44	0.34
	max	2	1.5	2	1.8

Table 2. Summary of operating conditions across the four trucks.

Since the inputs to the aftertreatment are unique for each truck, it is more challenging to attribute differences in tailpipe signals to aging as compared to the test-cell data.

2.3. Test-cell data vs Truck data

This section will compare some key aspects of the truck and the test-cell data and their implications for model-development and diagnostics:

1. **Aging signatures** In test-cell data, the two catalysts are clearly labeled as degreened and end-of-useful-life, whereas the aging levels on the four trucks are unknown. Also, the test-cell data has experiments where degreened and aged aftertreatment were run under identical operating conditions. Therefore, unlike truck data, differences in tailpipe signals for the two catalysts in test-cell data can be attributed to aging. Therefore, the test-cell data is more suitable for developing a model to capture aging.

2. **Available signals:** The test-cell data has DOC-out NO, NO_2, TP NH_3, TP NOx, and TP N_2O signals as compared to just the TP NOx signal in the truck data. It was shown in Subsection 2.1.2 that there are operating conditions where only a subset of these signals show aging signatures. Therefore, the test-cell data gives more insight about the effects of aging as compared to the truck data.

3. **Commercial NOx sensors vs FTIR:** Test-cell data has measurements from FTIR sensors, as opposed to the commercial NOx sensors in the truck data. Since the commercial NOx sensors have several limitations such as lower accuracy, cross-sensitivity to NH_3, and inability to operate below the light-off temperature, the FTIR measurements provide a more complete and cleaner data for modeling.

4. **On-road vs In-Lab Conditions:** Given the challenges with truck data, the test-cell data is clearly more suitable to build a model from scratch. However, the truck data provides great insights about the challenges posed by on-road conditions. These insights have played a key role in

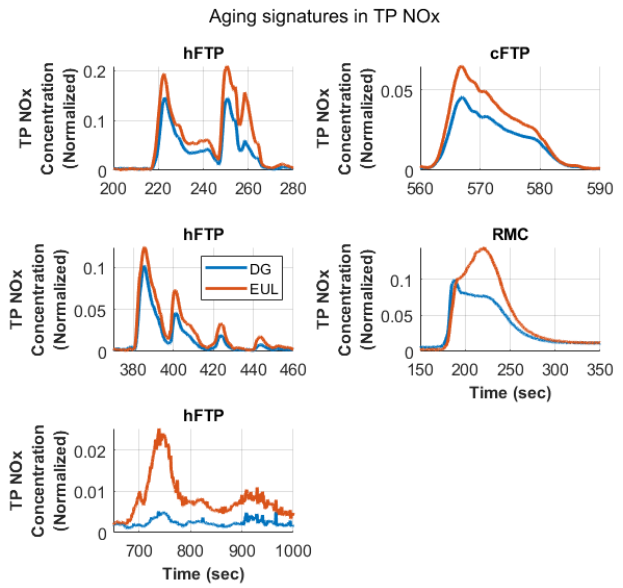

Figure 7. Aging signatures observed in tailpipe NOx for the three drive cycles. Note that the three subplots for hFTP, shown on the left side, are zoomed in sections from the same test.

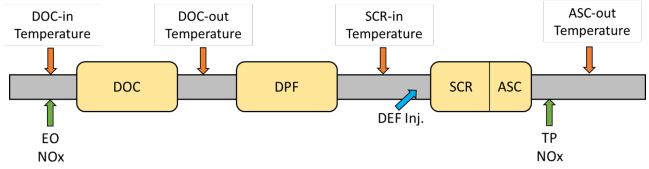

Figure 8. Exhaust layout with the sensors available on commercial trucks.

laying down the modeling requirements, which will be discussed in the next section.

3. THE SCR-ASC MODEL

3.1. Model Requirements

In this work, the model has been developed to primarily meet the following requirements:

1. **Accuracy requirement:** The model in this work is intended to be used for developing model-based diagnostic algorithm(s). To avoid false positives and false negatives, it is important to pick the right operating conditions to activate the diagnostic algorithm. Therefore, unlike a controller, a diagnostic method would not be running at all times and the model doesn't need to be accurate during operating conditions when the OBD would not be running.
   The model needs to be at its most accurate during operating conditions that are suitable for diagnostics such as the ones where we can see a clear aging signature, i.e.

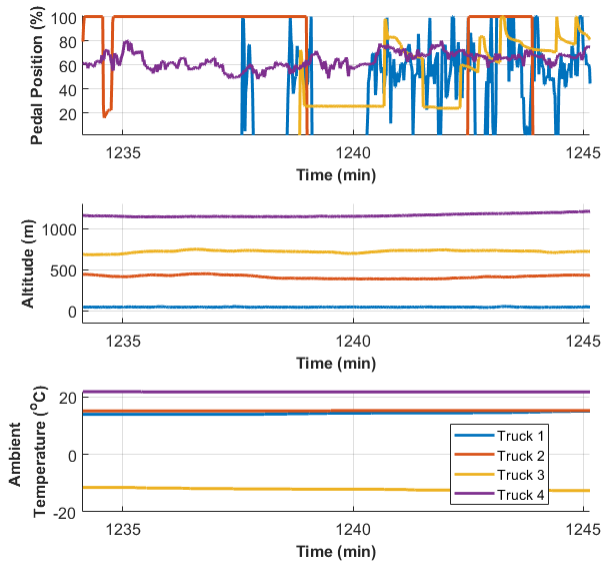

Figure 9. Segment of truck data showing differences in driving style and ambient conditions across the four trucks.

reasonable difference between EUL and degreened catalysts, for tailpipe NOx. But even under these operating conditions, the model doesn't need to capture the data accurately at each time-stamp of a drive cycle. Instead, the key requirement from a diagnostics-oriented model would be to capture the general trends in the tailpipe signals that occur as a result of aging.

2. **Ability to run with commercial sensors:** Apart from exhaust gas flow rate and temperature, commercial trucks only have engine-out and tailpipe NOx measurements. Therefore, it must be possible to run the model with just those measurements.
   Even though aging signatures were observed in DOC-out NO and NO_2 signals, DOC-out NOx will be used as the input to the model. This is because DOC-out NO and NO_2 signals are not available in commercial trucks, and a DOC model will be required to calculate DOC-out NO and NO_2. Since the focus of current work is SCR+ASC, the DOC dynamics will not be taken into account at this stage.
   Also, the outputs from the SCR+ASC model would be tailpipe NOx, NH_3, and N_2O concentration as these measurements are available in the test-cell data, and will be used to calibrate and validate the model. However, only the tailpipe NOx values will be used when testing the model on data from commercial trucks.

Model Objective: To summarize, the primary objective is to develop a diagnostics-oriented model for SCR+ASC that can capture aging signatures observed in the test-cell data with sensors available in commercial trucks.

3.2. Selective Catalytic Reduction (SCR)

The SCR catalyst is responsible for reducing engine-out NOx into harmless N_2 and H_2O. Diesel Exhaust Fluid (DEF), which is a mixture of 32.5% urea and 67.5% distilled water, is injected into the exhaust. Exhaust heat converts urea to NH_3, which is then adsorbed by the catalyst. Some of the adsorbed NH_3 reduces the NOx, and the rest gets desorbed or oxidized.

3.2.1. SCR Reactions

The Eley Rideal mechanism is widely accepted to be an accurate representation of the Urea-SCR reactions (Hsieh, 2010), (Yuan, Liu, & Gao, 2015). The key processes and corresponding chemical reactions in the Urea-SCR system as per the Eley Rideal mechanism are as follows:

1. Urea to NH_3 conversion.
   Thermolysis:

$$(NH_2)_2CO \longrightarrow HNCO + NH_3 \tag{1}$$

   Hydrolysis:

$$HNCO + H_2O \longrightarrow NH_3 + CO_2 \tag{2}$$

2. NH_3 adsorption and desorption.

$$NH_3 + \theta_{\text{free}} \longleftrightarrow NH_3(\text{ads}) \tag{3}$$

   where θ_{free} is the number of moles of catalyst sites available for NH_3 adsorption.
3. NOx reduction.
   Standard SCR reaction:

$$4\,NH_3(\text{ads}) + 4\,NO + O_2 \longrightarrow 4\,N_2 + 6\,H_2O \tag{4}$$

   Fast SCR reaction:

$$4\,NH_3(\text{ads}) + 2\,NO + 2\,NO_2 \longrightarrow 4\,N_2 + 6\,H_2O \tag{5}$$

   Slow SCR reaction:

$$8\,NH_3(\text{ads}) + 6\,NO_2 \longrightarrow 7\,N_2 + 12\,H_2O \tag{6}$$

   Slow reaction is usually ignored when writing the dynamic equations, as it is much slower than the fast and the standard reactions.
4. NH_3 oxidation.

$$4\,NH_3(\text{ads}) + 3\,O_2 \longrightarrow 2\,N_2 + 6\,H_2O \tag{7}$$

3.2.2. SCR Model

A high-fidelity model for the Urea-SCR system will require partial differential equations (PDEs) to represent chemical reactions, gas flow and convective heat transfer (Nova & Tronconi, 2014), (Yuan et al., 2015). However, such model would be computationally too expensive to be embedded in a micro-controller. Hence, several references such as (Hsieh, 2010), (Zhao, Chen, Hu, & Chen, 2015) and (Ofoli, 2014) have used a lumped parameter zero-dimensional model by treating the catalyst as a continuous stirred tank reactor (CSTR) as shown in Figure 10. The CSTR model assumes homogeneous distribution of reacting species in the catalyst which allows using ordinary differential equations (ODEs) instead of PDEs to model the Urea-SCR system dynamics.

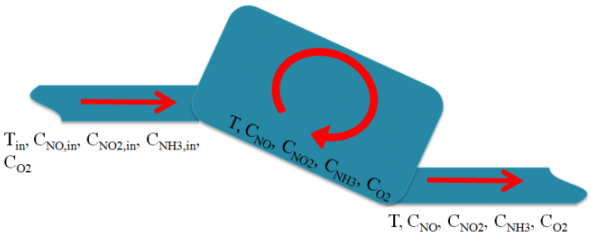

Figure 10. Schematic of the CSTR Model (Taken from (Hsieh, 2010)).

The system dynamic equations for the CSTR model can then be obtained using mass balance across the catalyst: depending on whether or not NO_2 dynamics are considered, the CSTR model can have three or four states, respectively. In this work, the three-state CSTR model will be used for SCR because the aftertreatment system on commercial trucks does not have any sensor to measure NO_2 concentration upstream or downstream of SCR. The system dynamic equations for the three-state CSTR models are given by Equation 8.

$$\begin{aligned}
\dot{x}_1 &= \frac{F}{V}(u_1 - x_1) - \alpha_{\text{ads}} x_1 (1 - x_3) K + \alpha_{\text{des}} x_3 K \\
\dot{x}_2 &= \frac{F}{V}(u_2 - x_2) - \alpha_{\text{SCR}}(x_2)(x_3 K) \\
\dot{x}_3 &= -\alpha_{\text{SCR}} x_2 x_3 + \alpha_{\text{ads}} x_1 (1 - x_3) - \alpha_{\text{des}} x_3 - \alpha_{\text{oxi}} x_3
\end{aligned} \tag{8}$$

The temperature (T) dependence of the reaction rates (α_i) and catalyst NH_3 storage capacity (K) is given by

$$\alpha_i = A_i e^{-\frac{E_i}{RT}}, K = \frac{S_1}{V} e^{-S_2 T} \tag{9}$$

And the urea to NH_3 conversion dynamics is given by

$$\dot{u}_1 = \frac{1}{\tau}(-u_1 + \eta_{\text{urea}} u_{1,\text{ideal}}) \tag{10}$$

All the symbols in Equations 8 to 10 are described in the Nomenclature section at the end of the paper.

3.3. Ammonia Slip Catalyst (ASC)

It is difficult to get low SCR-out NOx and NH_3 simultaneously. ASC is responsible for oxidizing the SCR-out NH_3 to N_2. Therefore, for the same amount of tailpipe NOx, an SCR-ASC system will have lower tailpipe NH_3 than an SCR-only system. However, the ASC is not perfect and it can oxidize some SCR-out NH_3 into NO and N_2O.

3.3.1. ASC Reactions

The key reactions in an ASC are as follows (Shrestha et al., 2016):

1. Conversion of NH_3 to N_2. This is the desired reaction.

$$4\,NH_3 + 3\,O_2 \longrightarrow 2\,N_2 + 6\,H_2O \tag{11}$$

2. Conversion of NH_3 to NO and N_2O. These are the undesired reactions.

$$4\,NH_3 + 5\,O_2 \longrightarrow 4\,NO + 6\,H_2O \tag{12}$$

$$2\,NH_3 + 2\,O_2 \longrightarrow N_2O + 3\,H_2O \tag{13}$$

3.3.2. ASC Model

An ODE model, with concentration of NH_3, NO, and N_2O as the three states, could be developed for ASC from the reactions 11 to 13 using mass balance and CSTR assumptions similar to the SCR model. Combining such model with the three-state SCR model would give us a six-state nonlinear ODE model for the SCR-ASC system. However, calibrating such model would be extremely difficult in the absence of SCR-out measurements. Therefore, instead of developing an ODE model for ASC, we have developed a look-up table model based on ASC's NH_3 conversion efficiency and selectivity to NOx and N_2O. Since the look-up table doesn't model ASC dynamics, it won't be able to capture the tailpipe signals accurately at each time-stamp in the drive cycles. However, the results will show that this model can capture the general trends caused due to aging, which should be sufficient for diagnostics as we discussed earlier and will also be demonstrated in the later sections.

ASC's NH_3 conversion efficiency and selectivities to NOx and N_2O can be calculated using the following equations:

$$\eta_{NH_3} = \frac{y_{NH_3,SCR} - y_{NH_3,TP}}{y_{NH_3,SCR}} \tag{14}$$

$$S_{NOx} = \frac{y_{NOx,TP} - y_{NOx,SCR}}{y_{NH_3,SCR} - y_{NH_3,TP}} \tag{15}$$

$$S_{N_2O} = \frac{2y_{N_2O,TP}}{y_{NH_3,SCR} - y_{NH_3,TP}} \tag{16}$$

where η_{NH_3} is ASC's NH_3 conversion efficiency and S_{NOx} and S_{N_2O} are selectivities to NOx and N_2O, respectively.

Figure 11 shows the curves for ASC's NH_3 conversion efficiency and sensitivities vs temperature and flow rate reported in (Shrestha et al., 2016). Since ASC's NH_3 conversion efficiency and sensitivities are functions of temperature and flow rate, two-dimensional look-up tables can be developed to calculate NH_3 conversion efficiency and sensitivities for any given combination of temperature and flow rate. Since we don't have detailed ASC-in and ASC-out data, it won't be possible to obtain the exact relation from temperature and flow rate to efficiency and selectivities. Therefore, our objective is to maintain the qualitative curves reported in (Shrestha et al., 2016) and manipulate them empirically using the existing test-cell data such that the SCR+ASC model can match the tailpipe signals.

The curves shown in Figure 11 are a good starting point to develop the look-up tables because the temperatures in these curves cover the range of values in the test-cell data. The space velocities given by (Shrestha et al., 2016) in Figure 11 are 66k-hr^{-1} and 265k-hr^{-1}, but these exact space velocity values are not important as the curves at these values will be manipulated to obtain the curves at three flow rate values within the range of our data. The range of exhaust volume flow rate in the data is from 0.04 m^3/sec to 0.6 m^3/sec. Curves for 66k-hr^{-1} will be manipulated to get selectivity vs temperature curves for a flow rate of 0.04 m^3/sec and 0.2 m^3/sec. And the curves for 265k-hr^{-1} will be manipulated to get selectivity vs temperature curves for the flow rate of 0.7 m^3/sec. This will be further elaborated in Section 3.4.1.

The step-by-step implementation of the ASC model, based on these 2D look-up tables, is given as follows:

1. For a given temperature (T), flow rate (F) calculate η_{NH_3}, S_{NOx}, and S_{N_2O} using the 2D look-up tables.

2. Calculate tailpipe NH_3 using η_{NH_3} and SCR-out NH_3.

$$y_{NH_3,TP} = (1 - \eta_{NH_3})\, y_{NH_3,SCR} \tag{17}$$

3. Calculate tailpipe NOx using S_{NOx}, SCR-out NOx, SCR-out NH_3, and tailpipe NH_3.

$$y_{NOx,TP} = y_{NOx,SCR} + S_{NOx}\,(y_{NH_3,SCR} - y_{NH_3,TP}) \tag{18}$$

4. Calculate tailpipe N_2O using S_{N_2O}, SCR-out NH_3, and tailpipe NH_3.

$$y_{N_2O,TP} = \frac{S_{N_2O}}{2}\,(y_{NH_3,SCR} - y_{NH_3,TP}) \tag{19}$$

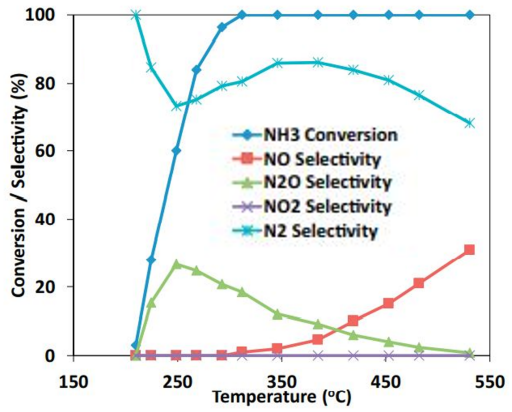

(a) 66k hr^{-1} space velocity

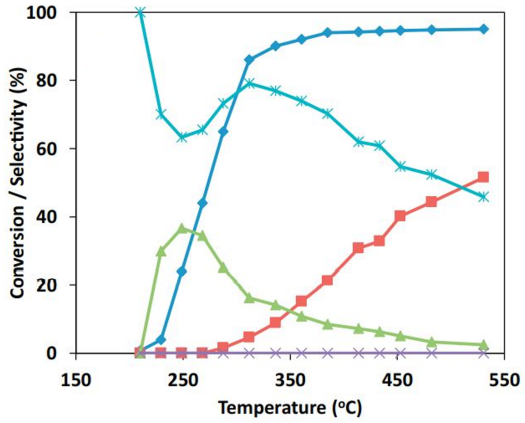

(b) 265k hr^{-1} space velocity

Figure 11. Dependence of ASC's NH_3 conversion efficiency and selectivities on temperature and flow rate, taken from (Shrestha et al., 2016)

.

3.4. Model Calibration

Figure 12 shows the combined SCR-ASC model. Inputs to the SCR model are: T, F, Engine-out NOx (u_{NOx}), and Injected DEF (u_{DEF}). Outputs from the SCR model and the inputs to the ASC model are SCR-out NH_3 ($y_{\text{NH}_3,\text{SCR}}$) and NOx ($y_{\text{NOx,SCR}}$). Tailpipe NH_3 ($y_{\text{NH}_3,\text{TP}}$), NOx ($y_{\text{NOx,TP}}$), and N_2O ($y_{\text{N}_2\text{O,TP}}$) are the outputs from the ASC model.

Hot FTP cycle (hFTP) data is used to calibrate the SCR and ASC models for both degreened and EUL catalysts. Cold FTP (cFTP) and RMC will be used for validation. Parameters for the SCR model are: Pre-exponential coefficients (A_i) and activation energies (E_i) for the reaction rates, storage capacity parameters S_1, S_2, Urea-to-NH_3 conversion efficiency (η_{urea}), and time constant for urea-to-NH_3 conversion (τ). Parametrization of the look-up tables for the ASC model will be discussed in Section 3.4.1.

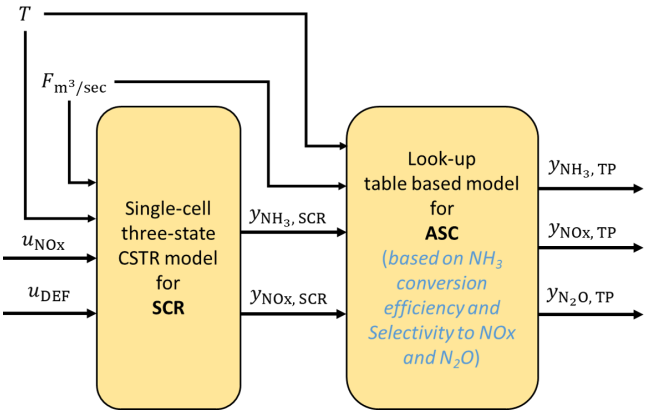

Figure 12. SCR+ASC model structure

3.4.1. Look-up tables for $S_{\text{N}_2\text{O}}$, η_{NH_3}, and S_{NOx}

Look-up table for $S_{\text{N}_2\text{O}}$: The step-by-step procedure to obtain the look-up table from temperature and flow rate to $S_{\text{N}_2\text{O}}$ is given as follows:

1. Extract $S_{\text{N}_2\text{O}}$ vs temperature data from Figure 11 for 66k hr^{-1} and 265k hr^{-1} space velocities. The values in Figure 11 are for the catalyst that was used in (Shrestha et al., 2016). Therefore, these are not necessarily the true selectivities for the catalyst used in this work. These will be used as initial guesses, and will be parametrized by offsetting the curves for $S_{\text{N}_2\text{O}}$ vs temperature in Figure 11. Let the initial values of $S_{\text{N}_2\text{O}}$ from Figure 11 be $S_{\text{N}_2\text{O,init66}}$ for 66k hr^{-1} space-velocity and $S_{\text{N}_2\text{O,init265}}$ for 265k hr^{-1} space-velocity. Then the look-up table for $S_{\text{N}_2\text{O}}$ can be parametrized as follows:

$$\begin{aligned} S_{\text{N}_2\text{O,lowflow}} &= S_{\text{N}_2\text{O,init66}} + p_1 \\ S_{\text{N}_2\text{O,midflow}} &= S_{\text{N}_2\text{O,init66}} + p_2 \\ S_{\text{N}_2\text{O,highflow}} &= S_{\text{N}_2\text{O,init265}} + p_3 \end{aligned} \tag{20}$$

   where $S_{\text{N}_2\text{O,lowflow}}$, $S_{\text{N}_2\text{O,midflow}}$, and $S_{\text{N}_2\text{O,highflow}}$ are the values of ASC's selectivity to N_2O at the three flow rates of 0.04 m^3/sec, 0.2 m^3/sec, and 0.7 m^3/sec, respectively.

2. After the first step, we have $S_{\text{N}_2\text{O}}$ values for several temperatures at each of the three flow rates. At each flow rate, $S_{\text{N}_2\text{O}}$ is calculated for other temperatures in hFTP using piece-wise cubic Hermite interpolation. Then for each temperature, $S_{\text{N}_2\text{O}}$ is calculated for other flow rates in hFTP using linear interpolation. Note that cubic interpolation is used to capture the nonlinear selectivity-vs-temperature curves in Figure 11, whereas linear interpolation is used for flow rate as we have selectivity values for only three flow rates, making it unnecessary and infeasible to use nonlinear interpolation.
3. After the second step, we have $S_{\text{N}_2\text{O}}$ values for many temperatures and flow rates. Then the temperature, flow rate and selectivity values are stacked

together to form a 2D interpolant using MATLAB's `scatteredInterpolant` function. This interpolant is the 2D look-up table that can calculate S_{N_2O} for any combination of temperature and flow rate.

Look-up table for η_{NH_3}: It is possible to obtain the look-up table for η_{NH_3} by extracting η_{NH_3} vs temperature data from Figure 11, and following a similar process to the look-up table for S_{N_2O}. However, as shown in Figure 13, the SCR-out NH_3 slip, calculated using η_{NH_3} vs temperature curves from Figure 11, is less than $y_{NH_3,TP} + 2y_{N_2O,TP}$. This would imply that $S_{N_2O} = 2y_{N_2O,TP}/(y_{NH_3,SCR} - y_{NH_3,TP}) > 1$, which is not possible. Therefore, the look-up table for η_{NH_3} is created

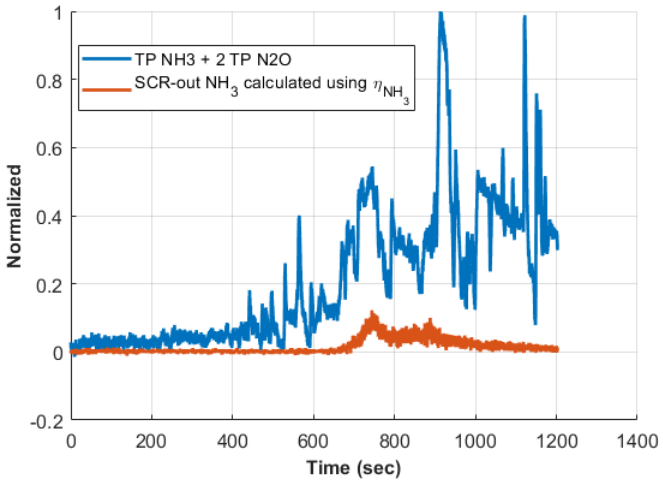

Figure 13. Comparison of $y_{NH_3,SCR}$, calculated using η_{NH_3}, and $y_{NH_3,TP} + 2y_{N_2O,TP}$.

using the following alternate approach:

1. At each time-stamp in hFTP, calculate SCR-out NH_3 using S_{N_2O}, tailpipe NH_3, and tailpipe N_2O using the following equation:

$$y_{NH_3,SCR} = y_{NH_3,TP} + \frac{2y_{N_2O,TP}}{S_{N_2O}} \tag{21}$$

2. Calculate η_{NH_3} from $y_{NH_3,SCR}$ and $y_{NH_3,TP}$ using Equation 14.
3. Stack temperature, flow rate, and η_{NH_3} at each time-stamp using `scatteredInterpolant` to obtain the look-up table from temperature and flow rate to η_{NH_3}.

Look-up table for S_{NOx}: S_{NOx} can be calculated from $y_{NH_3,SCR}$, $y_{NH_3,TP}$, $y_{NOx,SCR}$, and $y_{NOx,TP}$ using Equation 15. However, since test-cell data does not have SCR-out measurements, $y_{NOx,SCR}$ is unknown. Therefore, Equation 15 can be parametrized as follows:

$$S_{NOx} = \frac{p_4(y_{NOx,TP})}{y_{NH_3,SCR} - y_{NH_3,TP}} \tag{22}$$

where p_4 is the fraction of tailpipe NOx produced from NH_3 oxidation by ASC. This equation assumes that p_4 is a constant, which may not be true in general. However, this is a reasonable assumption to calculate approximate values of S_{NOx} for model calibration.

The look-up tables for both degreened and EUL catalysts were developed using these steps. Figure 14 shows the NH_3 conversion efficiency and selectivities vs temperature and flow rate, based on these look-up tables. Note that the curves for the degreened and EUL catalysts are generally very close to each other, which is a sanity check because the same S_{N_2O} vs temperature data was used for both degreened and EUL catalysts when creating the look-up table for S_{N_2O} and therefore it was expected that similar look-up tables will be obtained for both. The slight differences between the curves for degreened and EUL catalyst, shown in Figure 14, could be attributed to numerical differences caused due to slightly different operating conditions and tailpipe signals for the two catalysts.

Since these curves look qualitatively similar to the ones in Figure 11, these look-up tables could be used as reasonable initial guesses for the ASC model, which can be calibrated by tuning p_1, p_2, p_3, and p_4. Note that η_{NH_3}, S_{NOx}, and S_{N_2O} are zero below 200^{o}C, which is the threshold for ASC activation.

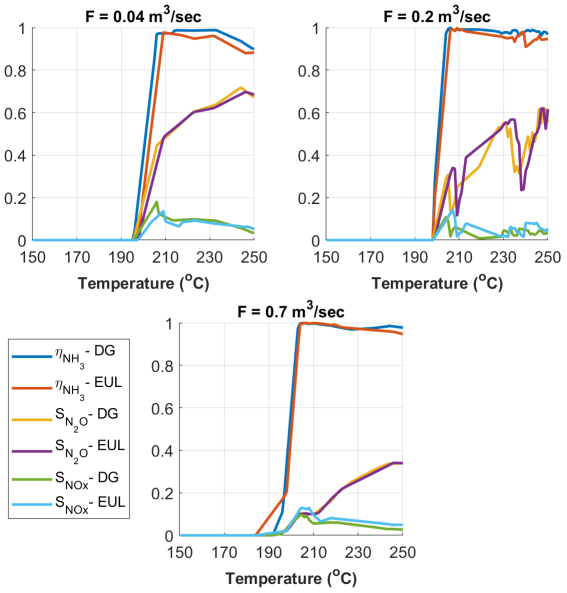

Figure 14. η_{NH_3}, S_{NOx}, and S_{N_2O} vs temperature and flow rate, based on the 2D look-up tables for degreened (DG) and EUL catalyst.

3.4.2. Current Calibration Approach for SCR+ASC Model

As mentioned earlier, hFTP is used to calibrate the SCR+ASC model. The following steps summarize the procedure to run the SCR+ASC model:

1. Integrate the three-state ODE Equations 8 to get SCR-out NH_3 and NOx.
2. Calculate η_{NH_3}, S_{NOx}, and S_{N_2O} at each time point using the look-up tables from T, F.
3. Calculate tailpipe NH_3 from η_{NH_3} and $y_{NH_3,SCR}$.
4. Calculate tailpipe NOx from S_{NOx}, $y_{NOx,SCR}$, $y_{NH_3,TP}$, and $y_{NH_3,SCR}$.
5. Calculate tailpipe N_2O from S_{N_2O}, $y_{NH_3,TP}$, and $y_{NH_3,SCR}$.

The parameters for the SCR-ASC model can be identified by solving the following optimization problem:

$$
\begin{aligned}
\min_{\theta_{SCR},\theta_{ASC}} \quad & J = \sum_{t=t_1}^{t_2} \left(e^2_{NH_3,TP} + e^2_{NOx,TP} + e^2_{N_2O,TP}\right) \\
\text{subject to} \quad & A_i, E_i, S_1, S_2 > 0 \\
& 0 < \eta_{urea} < 1 \\
& 0 < \tau < 50 \\
& -1 < p_1, p_2, p_3 < 1 \\
& 0 < p_4 < 1 \\
\text{where} \quad & \\
& e_{i,TP} = y_{i,TP} - \hat{y}_{i,TP} \\
& \theta_{SCR} = [A_i, E_i, S_1, S_2, \eta_{urea}, \tau] \\
& \theta_{ASC} = [p_1, p_2, p_3, p_4]
\end{aligned}
\tag{23}
$$

where $y_{i,TP}$ are the true tailpipe signals and $\hat{y}_{i,TP}$ are the model-out values. Also note that t_1 and t_2 denote the times during which clear aging signature was observed in hFTP data. This implies that we want good model accuracy only when the operating conditions are favorable for diagnostics.

The Trust-region-reflective algorithm, using MATLAB's `lsqnonlin`, was used to solve the optimization problem to obtain the fits shown in Figure 15.

Visually, the fits shown in Figure 15 are reasonable for all tailpipe signals. To quantify these fits, Table 3 shows the values of average modeling error in ppm and as a fraction (r_{mean}) of average value of the true signals. Note that the average error for tailpipe NOx and tailpipe NH_3 is less than 1 ppm for both DG and EUL catalysts. However, it is still 37% of the average value of true tailpipe NOx for the DG catalyst, which is around 2 ppm. The average error for tailpipe N_2O is around 0.2 ppm for the DG catalyst and around 6.4 ppm for the EUL catalyst, which is about 23% of the average value of true tailpipe N_2O. Average error values in Table 3 demonstrate that very low modeling error could still be a significant

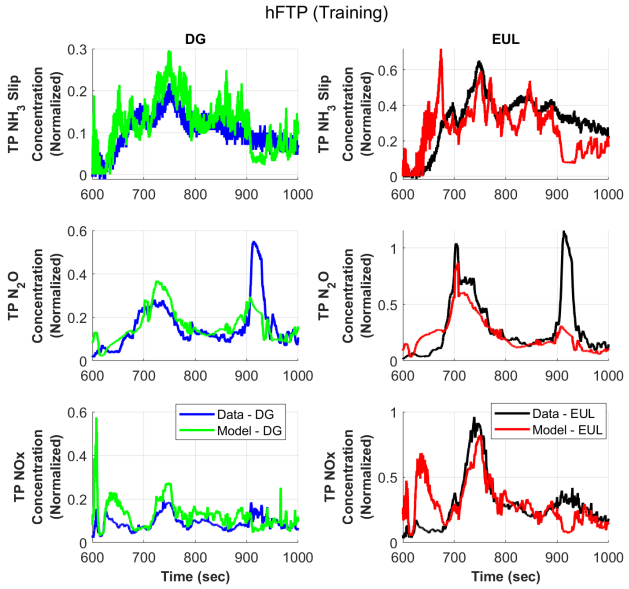

Figure 15. TP signal fits for degreened and EUL catalysts after calibrating the model on hFTP cycle.

fraction of the true signal value if the signal itself is small. But, it will be shown in Section 4 that a model-based diagnostic method could be designed to handle modeling error up to 10 ppm in tailpipe NOx. So, even if the modeling error is significant with respect to the true signal value, the model can be considered accurate enough for the OBD method in Section 4 to capture the aging signatures if the modeling error is less than 10 ppm.

One observation from Figure 15 is that the model is not able to capture the second spike in tailpipe N_2O between 900-950 seconds. The reason for this spike is not exactly clear at this point, but it could be due to conditions favoring NH_3 desorption, such as relatively low engine-out NOx, low flow rate and high exhaust temperature, leading to high SCR-out NH_3, which then gets primarily converted to tailpipe N_2O due to conditions where ASC's selectivity to N_2O is high. Our model's inability to capture this spike could primarily be attributed to the SCR model underestimating SCR-out NH_3 at that time. This will be analyzed more carefully in future to improve model calibration.

It should be noted that the pre-exponential coefficient, S_1, of the catalyst NH_3 storage capacity was the only free parameter when calibrating the model for the EUL catalyst. Therefore, the only difference between parameters for the degreened and the EUL catalysts is S_1. It is likely that other parameters, if left free, could also have taken different values for the EUL catalyst than the degreened one. But since the model could capture the trends due to aging by just changing S_1, it can be concluded that S_1 is adequate to capture the catalyst age.

	Avg Error ($\bar{e}$,ppm)		Avg True Value ($\bar{y}_{i,\text{TP}}$, ppm)		$r_{\text{mean}} = \frac{\bar{e}}{\bar{y}_{i,\text{TP}}}$	
	DG	EUL	DG	EUL	DG	EUL
TP NH_3	0.28	0.79	1.75	5.36	0.16	0.15
TP N_2O	0.23	6.43	14.37	27.67	0.01	0.23
TP NOx	0.67	0.12	1.83	5.81	0.37	0.02

Table 3. Average modeling error, in ppm and as a fraction (r_{mean}) of average value of the true signal, to quantify the tailpipe signal fits for hFTP shown in Figure 15.

However, the effect of other parameters could be explored in future work.

3.5. Model Validation

cFTP, RMC, and truck data are used to validate the SCR+ASC model. This section will present the model validation results on these data-sets.

3.5.1. Model Validation on cFTP Cycle

Figure 16 shows the validation fits for both degreened and EUL catalysts.

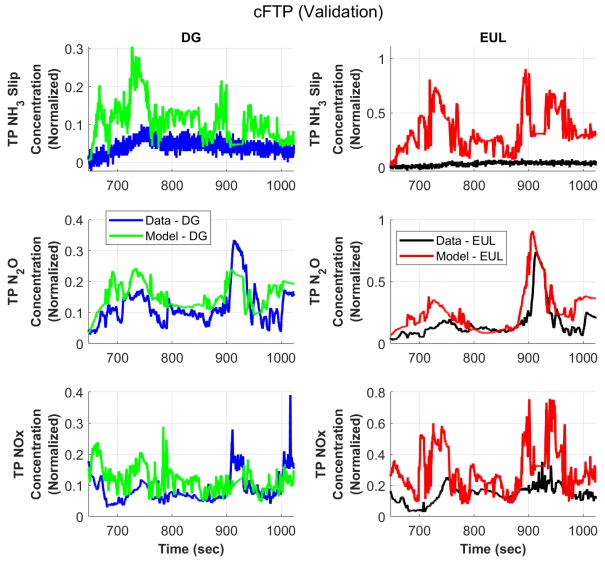

Figure 16. TP signal fits after ASC calibration for degreened and EUL catalysts for cFTP, which was used for validation.

Table 4 shows the average modeling error, in ppm and as a fraction (r_{mean}) of average value of the true signal, to quantify the validation fits shown in Figure 16. Very small values of true TP NH_3 signals lead to large r_{mean} values and bad visual fit for the EUL catalyst, but the fit is reasonable as the average error values are less than 10 ppm. Visual fits for TP N_2O and NOx are decent, supported by low average error values. Large r_{mean} values can again be attributed to small signal values.

	Avg Error ($\bar{e}$,ppm)		Avg True Value ($\bar{y}_{i,\text{TP}}$, ppm)		r_{mean}	
	DG	EUL	DG	EUL	DG	EUL
TP NH_3	4.2	8.1	0.6	0.5	6.39	17.31
TP N_2O	2.4	7	9.7	13.4	0.24	0.52
TP NOx	0.5	2.7	1.8	2.9	0.25	0.91

Table 4. Average modeling error, in ppm and as a fraction (r_{mean}) of average value of the true signal, to quantify the tailpipe signal fits for cFTP shown in Figure 16.

3.5.2. Model Validation on RMC Cycle

Ideally, the training data for the ASC look-up tables should cover a wider range of temperature and flow rate than the validation data because look-up tables can not extrapolate. However, the maximum temperature across the FTP cycles is 270^{o}C. But the temperature for the RMC cycle ranges from 260^{o}C to 350^{o}C. Therefore, the look-up tables in Figure 14 have to be extended for the RMC cycle by following the procedure in Section 3.4.1 using the ASC parameter values (p_1, p_2, p_3, p_4) obtained from calibrating the model on the hFTP cycle. Figure 17 shows the updated curves for NH_3 conversion efficiency and selectivities vs temperature and flow rate.

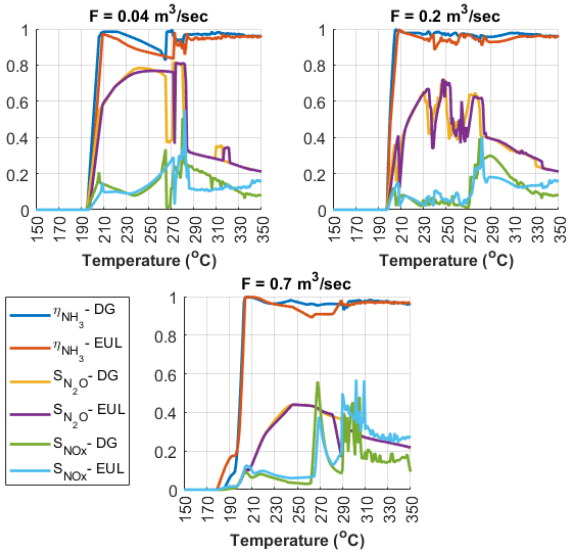

Figure 17. η_{NH_3}, S_{NOx}, and $S_{\text{N}_2\text{O}}$ vs temperature and flow rate, extended to RMC cycle.

Figure 18 shows that reasonable fits, quantified by low average error values in Table 5, were obtained for both degreened and EUL catalysts.

3.5.3. Model Validation on Truck Data

Since the duty cycles for the trucks are different to the cycles in test-cell data, the pre-exponential coefficient of the NOx re-

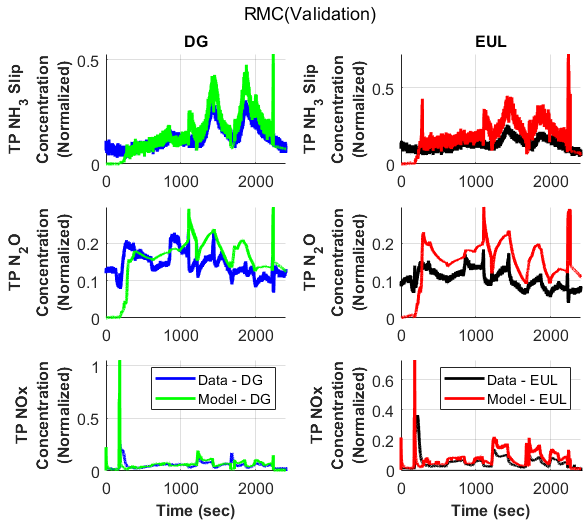

Figure 18. TP signal fits for degreened and EUL catalysts for RMC, which was used for model validation.

	Avg Error ($\bar{e}$,ppm)		Avg True Value ($\bar{y}_{i,\text{TP}}$, ppm)		r_{mean}	
	DG	EUL	DG	EUL	DG	EUL
TP NH_3	0.34	0.98	2.14	2.18	0.16	0.45
TP N_2O	0.93	3.81	13.03	9.42	0.07	0.40
TP NOx	1.52	5.52	15.42	15.79	0.1	0.35

Table 5. Average modeling error, in ppm and as a fraction (r_{mean}) of average value of the true signal, to quantify the tailpipe signal fits for RMC shown in Figure 18.

duction reaction (A_{SCR}) had to be adjusted to make the model work for truck data. Also, since the catalyst degradation levels on the trucks are unknown, the model is considered to be "performing reasonably" if any of the following conditions is satisfied:

1. The measured TP NOx is close to the TP NOx value estimated by the DG catalyst model, or
2. The measured TP NOx is close to the TP NOx value estimated by the EUL catalyst model, or
3. the measured TP NOx is more than the TP NOx value estimated by the DG catalyst model but less than the EUL catalyst model.

These conditions will be elaborated and quantified in the next section. Figure 19 shows an example of each of these conditions from the truck data. Table 6 shows that the model behaves reasonably, based on the three points mentioned above, for a significant number of points for all four trucks.

Using a simple cross-sensitivity model to improve the fits: Since the commercial tailpipe NOx sensor on the trucks is cross-sensitive to NH_3, the results in Table 6 could be improved by incorporating a simple model for cross-sensitivity.

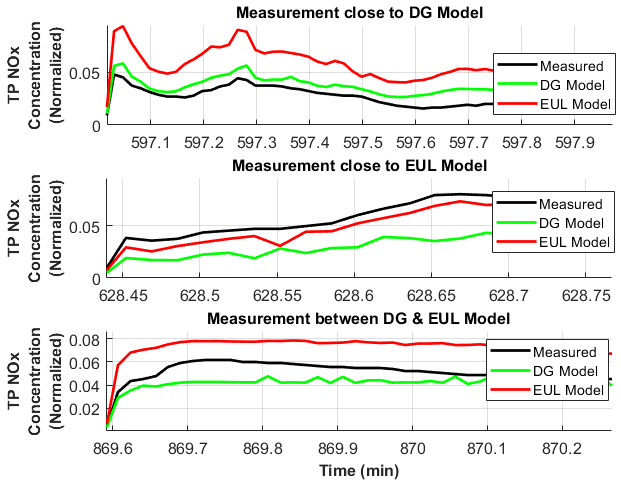

Figure 19. Examples from truck data where the model behaves reasonably.

	Truck 1	Truck 2	Truck 3	Truck 4
No. of points where T>200^oC	32036	57852	67500	55678
No. of points where model is reasonable	18515	47919	41591	24253
%. of points where model is reasonable	57.8%	82.8%	61.6%	43.5%

Table 6. Model performance on truck data quantified by the number and percentage of points where model behaves reasonably.

The tailpipe NOx and NH_3 values can be combined as follows to incorporate cross-sensitivity in both DG and EUL models:

$$y_{\text{NOx,cross}} = y_{\text{NOx,TP,model}} + \chi\left(y_{\text{NH}_3\text{,TP,model}}\right)$$

Though the cross-sensitivity factor χ can vary with temperature, it is a common approach to use a constant value for simplicity (Bonfils, Creff, Lepreux, & Petit, 2014; Hsieh & Wang, 2011; Schar, Onder, & Geering, 2006). It has been reported in (Hsieh & Wang, 2011) that the cross-sensitivity factor can range from 0 to 2. Therefore, in this paper, χ was varied from 0 to 2 for each truck to find the value that results in the best fit. Figure 20 shows that fits improved significantly for each truck by using this simple cross-sensitivity model with an appropriate χ. After incorporating cross-sensitivity, the percentage of points where the model is reasonable increased to 86.6%, 85.6%, 69.8%, and 80% for Trucks 1 to 4, respectively.

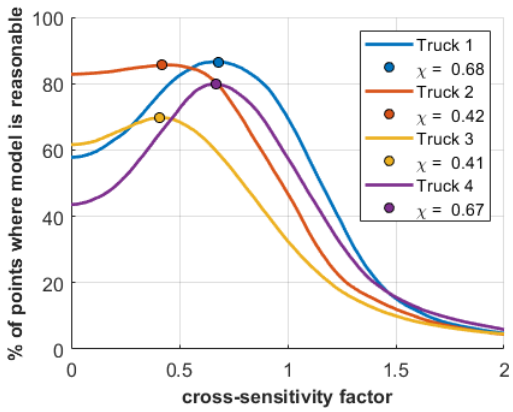

Figure 20. Percentage of points where the DG and EUL models behave reasonably for the truck data vs the cross-sensitivity factor χ.

The next section will discuss some model-based enable conditions applied to both test-cell and truck data.

4. MODEL-BASED OBD STRATEGY

In this section, we propose an OBD strategy based on our DG and EUL catalyst models. The key idea is to infer catalyst degradation level by comparing the measured tailpipe NOx to its value estimated by both DG and EUL models. The following sections will describe the enable conditions, precise diagnostic criteria, and results on both test-cell and truck data in detail.

4.1. Model-based Enable Conditions

Unlike a controller, OBD doesn't need to run at all times. It is important to pick the right conditions to activate the OBD. These conditions are called enable conditions. The enable conditions should minimize false positives and false negatives while maintaining a good In-use-performance-monitoring-ratio (IUMPR).

The fundamental objective of formulating enable conditions is to detect and pick operating conditions where a degraded catalyst would perform significantly differently to a degreened one. In other words, we need to pick operating conditions which are likely to produce aging signatures.

Since the OBD needs to detect catalyst degradation on commercial trucks using just tailpipe NOx measurements, we tried to find operating conditions in test-cell data where we see more than 10% difference in deNOx efficiency of the DG and the EUL catalysts.

However, observations from test-cell data, such as the one shown in Figure 21, showed that very similar operating conditions could lead to very different separability between DG and EUL catalysts based on %deNOx. Despite very similar values of DEF dosing, engine-out NOx, temperature, and flow rate, the difference between %deNOx of DG and EUL catalyst is more than 10% for the operating conditions plotted in blue and very small for the ones plotted in red. This shows that the separability between DG and aged catalysts depends not just on the present operating conditions but on the dynamics that happened in the past, which could be captured by a model. This establishes the importance of formulating model-based enable conditions.

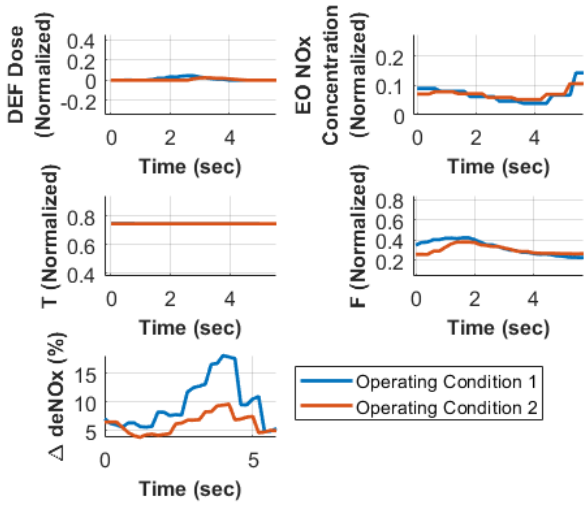

Figure 21. A section of test-cell data showing that very similar operating conditions could lead to different separability between DG and EUL catalysts based on %deNOx.

In this paper, we propose the following steps to pick operating conditions where aging signatures are expected to occur according to our model:

1. **Filter 1: Run both DG and EUL catalyst models** so that model-out TP NOx values could be compared to measured TP NOx. Since our model can't run at temperatures less than 200^{o}C, only the points where the SCR bed temperature is greater than 200^{o}C are selected in this step. Note that the data points are separated by 200 ms in the test-cell data and 1.2 seconds in the truck data.

2. **Filter 2:** From the points selected in step 1, **select points where the model behaves reasonably**, i.e.,at least one of the following conditions is satisfied:

$$
\begin{aligned}
&|y_{\text{NOx,TP,meas}} - y_{\text{NOx,TP,DG model}}| < 20 \text{ ppm OR} \\
&\frac{|y_{\text{NOx,TP,meas}} - y_{\text{NOx,TP,DG model}}|}{y_{\text{NOx,TP,meas}}} < 0.2 \text{ OR} \\
&|y_{\text{NOx,TP,meas}} - y_{\text{NOx,TP,EUL model}}| < 20 \text{ ppm OR} \\
&\frac{|y_{\text{NOx,TP,meas}} - y_{\text{NOx,TP,EUL model}}|}{y_{\text{NOx,TP,meas}}} < 0.2 \text{ OR} \\
&y_{\text{NOx,TP,DG model}} < y_{\text{NOx,TP,meas}} < y_{\text{NOx,TP,EUL model}} \text{ OR} \\
&y_{\text{NOx,TP,DG model}} < y_{\text{NOx,TP,EUL model}} < y_{\text{NOx,TP,meas}} - 20 \text{ OR} \\
&y_{\text{NOx,TP,DG model}} < y_{\text{NOx,TP,EUL model}} < 0.8 y_{\text{NOx,TP,meas}}
\end{aligned} \tag{24}
$$

Note that the first five conditions in Equation 24 quantify the three points listed in Section 3.5.3, which correspond to the catalysts with aging levels from DG to EUL. The last two conditions in Equation 24 were added to include catalysts that have degraded beyond EUL level. For the conditions in Equation 24, the threshold in modeling error is chosen to be 20 ppm or 20%, because the commercial NOx sensor has an uncertainty of 10 ppm or 10%, and the maximum average modeling error in tailpipe NOx across the three drive cycles was slightly less than 10 ppm. So, the measurement and modeling uncertainty were combined to choose 20 ppm or 20% as the threshold for this enable condition.

3. **Filter 3:** From the points selected after the first two steps, **select points where we expect to see difference in DG and EUL catalyst based on our model**. This can be quantified either based on %deNOx or TP NOx. For %deNOx-based filter 3, we select points where $(\eta_{\text{deNOx,DG model}} - \eta_{\text{deNOx,EUL model}}) > 10\%$. The threshold for %deNOx-based separation was chosen as 10% based on observations from test-cell data such that it is not too low to be affected by measurement or modeling errors and not too high to exclude a lot of points from the data.

   The other option for this enable condition is to quantify the separation in DG and EUL catalysts based on TP NOx, where we select points that satisfy all of the following conditions:

$$
\begin{aligned}
&y_{\text{NOx,TP,EUL model}} - y_{\text{NOx,TP,DG model}} > 20 \text{ ppm AND} \\
&\frac{y_{\text{NOx,TP,EUL model}} - y_{\text{NOx,TP,DG model}}}{y_{\text{NOx,TP,DG model}}} > 0.2 \text{ AND} \\
&\frac{y_{\text{NOx,TP,EUL model}} - y_{\text{NOx,TP,DG model}}}{y_{\text{NOx,TP,EUL model}}} > 0.2
\end{aligned} \tag{25}
$$

   Since the modeling error in tailpipe NOx for both DG and EUL catalyst models is up to 10 ppm, a difference of up to 20 ppm in $y_{\text{NOx,TP,DG model}}$ and $y_{\text{NOx,TP,EUL model}}$ could be because of modeling error. So, to ensure that the difference is due to an aging signature, 20 ppm or 20% was chosen as the threshold to quantify the separation based on tailpipe NOx.

4. **Filter 4:** From the points selected after the first three steps, **select points where the tailpipe NH_3 is too low for cross-sensitivity to significantly affect tailpipe NOx sensor readings.** In the existing literature, 2 is reported as the maximum cross-sensitivity factor (Hsieh & Wang, 2011). So, we select points where the tailpipe NOx sensor reading with maximum cross-sensitivity, $y_{\text{NOx}} + 2y_{\text{NH}_3}$, is not too different from the true reading, y_{NOx}, to affect the result of diagnostics. Therefore, this enable condition selects the points that satisfy the following conditions:

$$
\begin{bmatrix} 2y_{\text{NH}_3\text{,TP,DG model}} < 5 \text{ ppm} \\ \text{OR} \\ 2y_{\text{NH}_3\text{,TP,DG model}} < 0.05 y_{\text{NOx,TP,DG model}} \end{bmatrix}
$$

   AND

$$
\begin{bmatrix} 2y_{\text{NH}_3\text{,TP,EUL model}} < 5 \text{ ppm} \\ \text{OR} \\ 2y_{\text{NH}_3\text{,TP,EUL model}} < 0.05 y_{\text{NOx,TP,EUL model}} \end{bmatrix}
$$

   Since the goal of this enable condition is to select points where y_{NH_3} is too small for cross-sensitivity to affect the result of diagnostics, the threshold was chosen as 25% of the thresholds in Filter 2 and Filter 3.

4.2. Diagnostic criteria

For a perfect model and with perfect TP NOx measurements, we can expect the TP NOx measurements from a DG catalyst to overlap with the TP NOx estimated from the DG model. As the catalyst degrades, the TP NOx measurements will be higher than the value estimated by the DG model, and their difference will be higher for higher degradation. For an EUL catalyst, the measurement will overlap with the value estimated by the EUL model. However, there will be false positives and false negatives because of uncertainties in the model and imperfect measurements. This means that the TP NOx measurements can be closer to the DG model at some sample points and to the EUL model at others. However, if the enable conditions are designed effectively to minimize false positives and false negatives then the TP NOx measurements will align with the correct model according to the aging level. Based on this, we define the following diagnostic metric to be applied to the points selected after the four filters in Section 4.1.

The key idea in this metric is to classify each point, selected after applying the enable conditions, as either DG, EUL, or none. Let N_{DG} and N_{EUL} be the number of points classified as DG and EUL, respectively. Then the degradation level is quantified by the ratio of N_{EUL} to N_{DG}. Higher $N_{\text{EUL}}/N_{\text{DG}}$ would imply higher degradation.

The diagnostic metric classifies a point as DG if the measured TP NOx is closer to the value estimated by the DG model than the one by the EUL model, i.e.

$$|e_{\text{NOx,TP,DG model}}| < |e_{\text{NOx,TP,EUL model}}|,$$

where

$$e_{\text{NOx,TP,DG model}} = y_{\text{NOx,TP,meas}} - y_{\text{NOx,TP,DG model}}$$
$$e_{\text{NOx,TP,EUL model}} = y_{\text{NOx,TP,meas}} - y_{\text{NOx,TP,EUL model}}$$

Similarly, a point is classified as EUL if the measured TP NOx is closer to the value estimated by the EUL model than the one by the DG model, i.e.

$$|e_{\text{NOx,TP,DG model}}| > |e_{\text{NOx,TP,EUL model}}|$$

Note that every point is guaranteed to be classified as either DG or EUL by this metric.

Also note that this diagnostic metric is designed to compare the degradation level across various catalysts. Therefore, rather than giving an absolute aging level, it will give aging level relative to a baseline catalyst with known aging level.

4.3. Results with test-cell data

We will now apply the enable conditions in Section 4.1 to monitor both DG and catalysts during the three drive cycles in test-cell data:

1. **Filter 1**: We run both DG and EUL models for all three cycles, and only select points where SCR-bed temperature is greater than 200^{o}C.
2. **Filter 2**: We then select the points where the model behaves reasonably. Table 7 shows that this filter removes less than 5% of the points selected after the first filter. This implies that the model behaves reasonably in all three cycles for almost every point where the temperature is greater than 200^{o}C, which is expected as we saw good agreement between test-cell data and models.
3. **Filter 3**: From the points selected after applying the first two filters, this filter selects the points where aging signature can be expected based on DG and EUL catalyst models. This can be quantified either based on %deNOx efficiency or TP NOx from DG and EUL models. Table 7 shows that this filter removes most of the points. Based on %deNOx, very few but non-zero number of points are selected from all three cycles. However, no points are selected from cFTP and hFTP cycles if the filter is applied based on TP NOx.
4. **Filter 4**: This filter selects points where the TP NH_3, from both EUL and DG catalysts, is too low for cross-sensitivity to affect the OBD results. Over the three drive cycles, this filter removed 78% of the points selected after %deNOx-based filter 3 and no points were selected from the RMC cycle. When applied to the points selected after TP NOx-based filter 3, only 1.2% of the points got selected after this filter. In this case, all the selected points are from RMC because the TP NOx-based filter 3 removed all points from cFTP and hFTP.

		cFTP		hFTP
		DG	EUL	DG
Total no. of points		6014	6013	6012
Filter 1: No. of points where T>200^oC		2864	2885	3173
Filter 2: No. of points where model is reasonable		2863	2885	3170
Filter 3: No. of points where aging signature is expected based on DG and EUL models	Based on %deNOx	37	55	138
	Based on TP NOx	0	0	0
Filter 4: No. of points where TP NH_3 is too low for cross-sensitivity	after %deNOx-based filter 3	8	0	55
	after TP NOx-based filter 3	0	0	0

		hFTP	RMC	
		EUL	DG	EUL
Total no. of points		6012	12005	12005
Filter 1: No. of points where T>200^oC		3177	12005	12005
Filter 2: No. of points where model is reasonable		3174	11917	11907
Filter 3: No. of points where aging signature is expected based on DG and EUL models	Based on %deNOx	38	18	46
	Based on TP NOx	0	1177	879
Filter 4: No. of points where TP NH_3 is too low for cross-sensitivity	after %deNOx-based filter 3	9	0	0
	after TP NOx-based filter 3	0	1	24

Table 7. Number of points selected in test-cell data after applying the enable conditions

After filtering the data using enable conditions, the diagnostic metric was applied to the selected points. Table 8 shows that the diagnostic metric correctly classified all points from the DG catalyst as DG for all three cycles, resulting in $N_{\text{EUL}}/N_{\text{DG}} = 0$. For the EUL catalyst, this metric correctly classified 22 points as EUL out of 24 points selected from the RMC cycle by TP NOx-based enable conditions, resulting in $N_{\text{EUL}}/N_{\text{DG}} = 22/2 = 11$. However, this metric incorrectly classified all 9 points selected from hFTP by %deNOx-based enable conditions as DG for the EUL catalyst. These results

were combined over the three drive cycles and are shown in Table 9. Table 9 shows that %deNOx-based enable conditions selected 72 points whereas only 25 points were selected by TP NOx-based enable conditions. None of the enable conditions resulted in false positives, i.e., DG catalyst identified as EUL. For %deNOx-based enable conditions, 9 out of 72 points resulted in false negatives, i.e., EUL catalyst reported as DG, and only 2 out of 25 points for TP NOx-based enable conditions resulted in false negatives. These results show that the TP NOx-based enable conditions are more selective and hence more robust to false negatives.

		cFTP	
		DG	EUL
%deNOx-based enable conditions	Points selected	8	0
	$N_{\text{EUL}}/N_{\text{DG}}$	0/8	0/0
TP NOx-based enable conditions	Points selected	0	0
	$N_{\text{EUL}}/N_{\text{DG}}$	0/0	0/0

		hFTP	
		DG	EUL
%deNOx-based enable conditions	Points selected	55	9
	$N_{\text{EUL}}/N_{\text{DG}}$	0/55	0/9
TP NOx-based enable conditions	Points selected	0	0
	$N_{\text{EUL}}/N_{\text{DG}}$	0/0	0/0

		RMC	
		DG	EUL
%deNOx-based enable conditions	Points selected	0	0
	$N_{\text{EUL}}/N_{\text{DG}}$	0/0	0/0
TP NOx-based enable conditions	Points selected	1	24
	$N_{\text{EUL}}/N_{\text{DG}}$	0/1	22/2

Table 8. Results of applying diagnostic metric to the test-cell data selected after applying the enable conditions.

Testing OBD method's robustness to cross-sensitivity: Since the OBD has to work with commercial NOx sensors on trucks, it is important to test its robustness to cross-sensitivity. The cross-sensitivity factor can change as a function of other signals such as temperature, but the worst-case scenario was simulated in test-cell data by using the maximum possible value of 2 for the cross-sensitivity factor. Therefore, cross-sensitivity was simulated in test-cell data by combining the tailpipe NOx and NH_3 measurements using the following equation:

$$y_{\text{NOx,cross}} = y_{\text{NOx,TP,meas}} + 2y_{\text{NH}_3\text{,TP,meas}}$$

Then instead of $y_{\text{NOx,TP,meas}}$, $y_{\text{NOx,cross}}$ was compared to model-out TP NOx when applying the enable conditions and the diagnostic metric. Table 9 shows that almost identical results were obtained with the cross-sensitive NOx signal as well, suggesting that the enable conditions and the diagnostic metric are robust to cross-sensitivity.

%deNOx-based enable conditions	No cross-sensitivity	Cross-sensitive signal
Points selected	72	72
Correctly identified as DG	63	63
False positive (DG identified as EUL)	0	0
Correctly identified as EUL	0	0
False negative (EUL identified as DG)	9	9

Tailpipe NOx-based enable conditions	No cross-sensitivity	Cross-sensitive signal
Points selected	25	25
Correctly identified as DG	1	1
False positive (DG identified as EUL)	0	0
Correctly identified as EUL	22	23
False negative (EUL identified as DG)	2	1

Table 9. OBD results combined over the three drive-cycles for a clean and a cross-sensitive tailpipe NOx sensor reading.

4.4. Results with truck data

Table 10 shows the number of points selected from each truck after applying the enable conditions. Similar to test-cell data, filter 2 removed very few points (less than 7% of the points selected after filter 1) from the truck data as well. Filter 3, which selects the points where aging signature can be expected based on DG and EUL catalyst models, removed a significant number of points as it did for test-cell data. Based on %deNOx, filter 3 selected less than 0.6% of the points remaining after filter 2 from all four trucks. It was less restrictive based on tailpipe NOx as up to 28% of the points were selected. For the points selected after %deNOx-based filter 3, the cross-sensitivity based filter 4 selected 64% of the points. And it selected 60% of the points selected after TP NOx-based filter 3.

Table 11 shows the results of applying the diagnostic metrics to points selected from both %deNOx-based and tailpipe NOx-based enable conditions. Figure 22 shows $N_{\text{EUL}}/N_{\text{DG}}$ vs the number of miles on each truck. Higher $N_{\text{EUL}}/N_{\text{DG}}$ implies higher degradation, therefore Figure 22 shows the aging

		Truck 1	Truck 2
Total no. of points		33834	66133
Filter 1: No. of points where T>200^oC		32036	57852
Filter 2: No. of points where the model is reasonable		30900	55576
Filter 3: No. of points where aging signature is expected based on DG and EUL models	Based on %deNOx	73	145
	Based on TP NOx	952	537
Filter 4: No. of points where TP NH_3 is too low for cross-sensitivity	after %deNOx-based filter 3	28	130
	after TP NOx-based filter 3	629	462

		Truck 3	Truck 4
Total no. of points		79987	69848
Filter 1: No. of points where T>200^oC		67500	55678
Filter 2: No. of points where the model is reasonable		63136	54142
Filter 3: No. of points where aging signature is expected based on DG and EUL models	Based on %deNOx	398	193
	Based on TP NOx	17947	4291
Filter 4: No. of points where TP NH_3 is too low for cross-sensitivity	after %deNOx-based filter 3	212	148
	after TP NOx-based filter 3	10563	2727

Table 10. Number of points selected in truck data after applying the enable conditions

trends reported by the diagnostic metrics vs the number of miles on each truck.

Since we don't know the actual degradation levels on these trucks, the results can't be validated yet. However, it is encouraging that the diagnostic metric gave almost identical trends for both types of enable conditions. The only difference between the two trends is that the truck with 484k miles is reported to be more aged than the one with 271k miles for %deNOx-based enable conditions and vice versa for TP NOx-based enable conditions. This is because factors such as DPF regeneration, and different driving styles could result in higher degradation on a truck with lesser miles on it. Another consistent result from both enable conditions is that the truck with 711 kmiles is reported to be have the highest degradation among the four trucks. Even though these results could not be validated yet, mostly similar and sensible trends using different enable conditions increase the confidence in the relative aging levels, and is an encouraging result.

		Truck 1	Truck 2
%deNOx-based enable conditions	Points selected	28	130
	$N_{\text{EUL}}/N_{\text{DG}}$	1/27	87/43
TP NOx-based enable conditions	Points selected	629	462
	$N_{\text{EUL}}/N_{\text{DG}}$	332/297	335/127

		Truck 3	Truck 4
%deNOx-based enable conditions	Points selected	212	148
	$N_{\text{EUL}}/N_{\text{DG}}$	116/96	98/50
TP NOx-based enable conditions	Points selected	10563	2727
	$N_{\text{EUL}}/N_{\text{DG}}$	3866/6697	2110/617

Table 11. Results of applying diagnostic metrics to the truck data selected after applying the enable conditions based on %deNOx and tailpipe NOx.

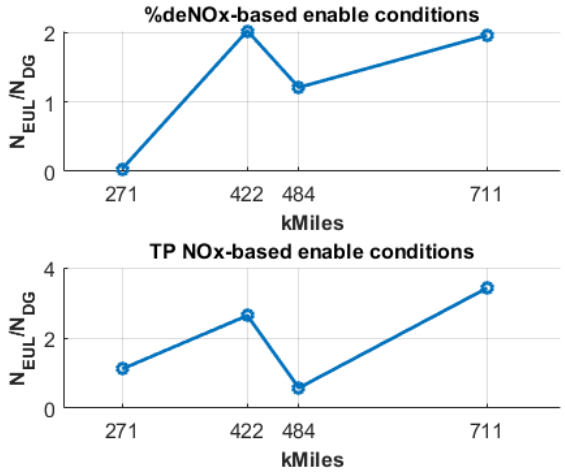

Figure 22. Aging trends reported by diagnostic metrics vs the number of miles on each truck. Higher $N_{\text{EUL}}/N_{\text{DG}}$ implies higher degradation

5. CONCLUSION AND FUTURE WORK

This paper presented a diagnostics-oriented SCR-ASC model and a model-based OBD method applied to both test-cell data and on-road data from commercial trucks. The standard three-state single-cell ODE model, based on CSTR assumption, was used to model SCR. The ASC was modeled as 2D look-up tables to determine ASC's NH_3 conversion efficiency, and selectivity to NOx and N_2O as a function of temperature and flow rate. Even though the look-up tables don't model ASC dynamics, the SCR-ASC model is shown to be capable of capturing the trends in tailpipe signals caused due to aging in the test-cell data and work reasonably for a significant portion of on-road data from commercial trucks, when combined with a simple model for commercial NOx sensor's cross-sensitivity to NH_3.

Based on this model, an OBD method with model-based enable conditions has been formulated and applied to both test-cell and truck data with commercial NOx sensors. Results of applying these enable conditions demonstrate the difficulty of robust SCR monitoring due to the trade-off between the number of points where the enable conditions are satisfied and the robustness of the diagnostics results to uncertainties. Increasing the robustness would result in more restrictive enable conditions.

Results on test-cell data show that the OBD gets enabled at very few points, which may not provide enough monitoring time to robustly diagnose an SCR-ASC system. But the majority of points selected in the test-cell data are correctly classified as DG or EUL with zero false positives and very few false negatives. The method is also shown to be robust to NOx sensor's cross-sensitivity to NH_3 when the tailpipe NOx and NH_3 signals in test-cell data were combined to simulate worst-case cross-sensitivity. However, a major limitation of the diagnostics-oriented model, combined with the diagnostics approach, is that it gets enabled at very few number of points in the test-cell data. This will be addressed in future by using a stochastic OBD method that quantifies the uncertainty propagation from the model to the diagnostic results.

It was demonstrated that this method could be implemented on commercial trucks with limited sensors. In the truck data, the enable conditions were satisfied at many more number of points than the test-cell data. Results on truck data show encouraging trends between relative degradation level and the number of miles on the four trucks. However, the diagnostic results on truck-data could not be validated at this stage because the aging levels on these trucks are unknown. In future, more data from commercial trucks with known aging levels will be used to validate and improve the model-based OBD method.

ACKNOWLEDGMENTS

We would like to thank Cummins Inc. for providing data and funding for this work, and Dr. Lyle Kocher from Cummins Inc. for technical guidance and support for this work. We would also like to thank Dr. Michael Haas from Cummins Inc., and Jagdish Hiremath for technical guidance during this work.

NOMENCLATURE

A_i	Pre-exponential coefficient for reaction i
E_i	Activation energy for reaction i in J/mol
F	Exhaust gas volume flow rate in m^3/sec
K	SCR Catalyst NH_3 storage capacity in moles
R	Universal gas constant in J/mol-K
S_{NOx}	ASC's selectivity to NOx
$S_{\text{N}_2\text{O}}$	ASC's selectivity to N_2O
T	Catalyst bed temperature in K
u_1	Concentration of injected NH_3 in mol/m^3
$u_{1,\text{ideal}}$	Ideal u_1 assuming instant and 100% conversion from urea to NH_3
u_2	Concentration of SCR-in NOx in mol/m^3
V	Catalyst volume in m^3
x_1	Concentration of SCR-out NH_3 slip in mol/m^3
x_2	Concentration of SCR-out NOx in mol/m^3
x_3	Fraction of SCR catalyst storage capacity occupied by NH_3
α_{ads}	Reaction rate for NH_3 adsorption to SCR catalyst
α_{des}	Reaction rate for NH_3 desorption from SCR catalyst
α_{oxi}	Reaction rate for oxidation of adsorbed NH_3 in SCR catalyst
α_{SCR}	Reaction rate for NOx reduction by adsorbed NH_3 in SCR catalyst
η_{NH_3}	ASC's NH_3 conversion efficiency
η_{urea}	Urea to NH_3 conversion efficiency
τ	Time-constant for Urea to NH_3 conversion

REFERENCES

Bonfils, A., Creff, Y., Lepreux, O., & Petit, N. (2014). Closed-loop control of a scr system using a nox sensor cross-sensitive to nh3. *Journal of Process Control*, *24*(2), 368–378.

Carb approves heavy-duty obd amendments, adopts real nox and co2 tracking [Computer software manual]. (2018 (accessed Nov 30, 2021)). (`https://dieselnet.com/news/2018/11carb.php`)

Chen, P., & Wang, J. (2016). Estimation and adaptive nonlinear model predictive control of selective catalytic reduction systems in automotive applications. *Journal of Process Control*, *40*, 78–92.

Daya, R., Desai, C., & Vernham, B. (2018). Development and validation of a two-site kinetic model for nh 3-scr over cu-ssz-13. part 1. detailed global kinetics development based on mechanistic considerations. *Emission Control Science and Technology*, *4*(3), 143–171.

Daya, R., Joshi, S. Y., Luo, J., Dadi, R. K., Currier, N. W., & Yezerets, A. (2020). On kinetic modeling of change in active sites upon hydrothermal aging of cu-ssz-13. *Applied Catalysis B: Environmental*, *263*, 118368.

Devarakonda, M., Parker, G., Johnson, J. H., Strots, V., & Santhanam, S. (2008). *Adequacy of reduced order models for model-based control in a urea-scr aftertreatment system* (Tech. Rep.). SAE Technical Paper.

Emissions Compliance, A. R., & Science Division, C. (2018 (accessed Nov 30, 2021)). Workshop for 2018 hd obd regulations update [Computer software manual]. (`https://ww2.arb.ca.gov/sites/default/files/classic/msprog/`

obdprog/hdobd_2017wspresentation.pdf)

Hsieh, M.-F. (2010). *Control of diesel engine urea selective catalytic reduction systems* (doctoral dissertation). The Ohio State University.

Hsieh, M.-F., & Wang, J. (2011). Development and experimental studies of a control-oriented scr model for a two-catalyst urea-scr system. *Control Engineering Practice*, *19*(4), 409–422.

Hu, J., Zeng, J., & Wei, L. (2018). Failure diagnosis and tolerant control method for hydrothermally aged scr system by utilizing ekf observer and mrac controller. *Energy*, *156*, 103–121.

Hu, J., Zeng, J., Wei, L., & Yan, F. (2017). Improving the diagnosis accuracy of hydrothermal aging degree of v2o5/wo3–tio2 catalyst in scr control system using an gs–pso–svm algorithm. *Sustainability*, *9*(4), 611.

Jiang, K., Yan, F., & Zhang, H. (2019). Hydrothermal aging factor estimation for two-cell diesel-engine scr systems via a dual time-scale unscented kalman filter. *IEEE Transactions on Industrial Electronics*, *67*(1), 442–450.

Ma, Y., & Wang, J. (2017). Observer-based estimation of aging condition for selective catalytic reduction systems in vehicle applications. *Journal of Dynamic Systems, Measurement, and Control*, *139*(2), 021002.

Matsumoto, A., Furui, K., Ogiso, M., & Kidokoro, T. (2016). *Model-based obd logic utilizing adsorption and desorption model of nh 3 in scr catalyst* (Tech. Rep.). SAE Technical Paper.

Nova, I., & Tronconi, E. (2014). *Urea-scr technology for denox after treatment of diesel exhausts*. Springer.

Ofoli, A. R. (2014). Experimental demonstration of ammonia storage and slip modeling with control for an scr aftertreatment system. *IEEE Transactions on Industry Applications*, *50*(4), 2342–2348.

Romijn, M., & Kumar, U. (2018 (accessed Nov 30, 2021)). California hd obd program—summary of 2018 amendments [Computer software manual]. (https://dieselnet.com/news/2018/12obd.php)

Schär, C. M., Onder, C. H., Geering, H., & Elsener, M. (2004). *Control-oriented model of an scr catalytic converter system* (Tech. Rep.). SAE Technical Paper.

Schar, C. M., Onder, C. H., & Geering, H. P. (2006). Control of an scr catalytic converter system for a mobile heavy-duty application. *IEEE Transactions on Control Systems Technology*, *14*(4), 641–653.

Shrestha, S., Harold, M. P., Kamasamudram, K., Kumar, A., Olsson, L., & Leistner, K. (2016). Selective oxidation of ammonia to nitrogen on bi-functional cu–ssz-13 and pt/al2o3 monolith catalyst. *Catalysis Today*, *267*, 130–144.

Surenahalli, H. S. (2013). *Dynamic model based state estimation in a heavy duty diesel aftertreatment system for onboard diagnostics and controls* (Unpublished doctoral dissertation). Michigan Technological University.

Upadhyay, D., & Van Nieuwstadt, M. (2002). Modeling of a urea scr catalyst with automotive applications. In *Asme international mechanical engineering congress and exposition* (Vol. 36290, pp. 707–713).

Yuan, X., Liu, H., & Gao, Y. (2015). Diesel engine scr control: current development and future challenges. *Emission Control Science and Technology*, *1*(2), 121–133.

Zhao, J., Chen, Z., Hu, Y., & Chen, H. (2015). Urea-scr process control for diesel engine using feedforward-feedback nonlinear method. *IFAC-PapersOnLine*, *48*(8), 367–372.